Jurnal Teknologi

Full Paper

COMPARATIVE STUDY OF CONFIGURATIONS FOR PHOTOVOLTAIC-THERMOELECTRIC GENERATOR COGENERATION SYSTEM

Razman Ayop[a]*, Chee Wei Tan[a], Shahrin Md Ayob[a], Lau Kwan Yiew[a], Ho Wai Shin[b]

[a]Faculty of Electrical Engineering, Universiti Teknologi Malaysia, 81310, Johor, Malaysia
[b]Faculty of Chemical and Energy Engineering, Universiti Teknologi Malaysia, 81310, Johor, Malaysia

Article history
Received
13 April 2023
Received in revised form
10 June 2023
Accepted
10 June 2023
Published Online
21 August 2023

*Corresponding author
razman.ayop@utm.my

Graphical abstract

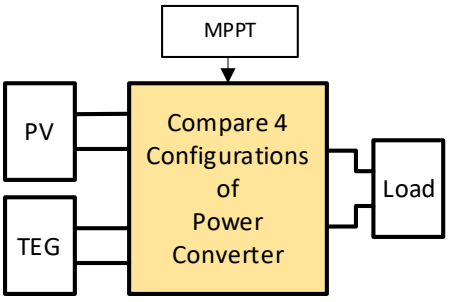

Abstract

Photovoltaic (PV) converts solar energy to electrical energy directly. During this process, the PV produce energy losses in the form of heat energy. To improve the system's efficiency, this heat energy is converted into electrical energy using the thermoelectric generator (TEG). The PV and TEG have a nonlinear current-voltage characteristic and it requires a power converter with maximum power point tracking (MPPT) to properly extract the energy. There are several configurations of power converters available for the PV-TEG cogeneration system (PTCS). Nonetheless, the literature that compares the performance of the configurations is unavailable. This paper compares 4 configurations for the PTCS, which include the separate boost full MPPT (SBFM), separate boost partial MPPT, series source boost MPPT, and PV boost MPPT with series TEG. The boost converter with perturb and observe MPPT method is used for all configurations to ensure a fair comparison. The results show that SBFM can efficiently extract the energy from both PV and TEG up to 98.5%. The other configurations can efficiently extract energy from the PV (more than 98.5%). However, the energy extracts from the TEG have a low efficiency down to 87%. Overall, the configuration chosen for the PTCS affects the efficiency of the system.

Keywords: PV, TEG, MPPT, P&O, boost converter

Abstrak

Fotovoltaik (PV) boleh menukarkan tenaga solar kepada tenaga elektrik secara terus. Semasa proses ini, PV menghasilkan tenaga hilang dalam bentuk tenaga haba. Untuk meningkatkan kecekapan sistem, tenaga haba ini ditukarkan kepada tenaga elektrik dengan menggunakan generator thermoelektrik (TEG). PV dan TEG tidak mempunyai karektar arus-voltan yang lurus dan ianya memerlukan pengubah kuasa dengan pencari hujung kuasa maxima (MPPT) untuk membolehkan penghasilan tenaga yang berkesan. Terdapat beberapa konfigurasi pengubah kuasa yang ada untuk sistem kogenerasi PV-TEG (PTCS). Tetapi, tiada literasi yang membandingkan prestasi konfigurasi ini. Kertas kajian ini membincangkan 4 konfigurasi untuk PTCS, iaitu galak asing MPPT penuh (SBFM), galak asing separa MPPT (SBPM), sumber selari galak MPPT, dan galak PV MPPT dengan TEG selari. Pengubah galak dengan MPPT ganggu dan perhati digunakan untuk semua konfigurasi untuk memastikan perbandingan yang dibuat adil. Keputusan menunjukkan SBFM dapat mengeluarkan tenaga daripada PV dan TEG secara berkesan sehngga 98.5%. Konfigurasi yang lain boleh mengeluarkan tenaga dari PV dengan berkesan (lebih 98.5%). Tetapi, prestasi pengeluaran tenaga daripada TEG jatuh serendah 87%. Secara keseluruhannya, konfigurasi yang dipilih untuk PTCS mempengaruhi kecekapas sistem tersebut.

Kata kunci: PV, TEG, MPPT, P&O, pengubah galak

1.0 INTRODUCTION

Renewable energy has become the focus of the world due to the advancement in the technology and threat of climate change. According to the Renewable 2023 Global Status Report, there is an average of 4.7% growth of renewable energy each year globally [1]. One of the renewable energies included in the growth is photovoltaic (PV). It is estimated that 78 GW of generation system is installed in 2021. The PV research has improved tremendously throughout the year. The focus of research is mainly focused on improving the performance of maximum power point tracking (MPPT). Since the PV current-voltage (I-V) characteristic curve is nonlinear, the MPPT is needed to extract the maximum power from the PV. The common MPPT method is the perturb and observe (P&O) method [2, 3]. This method is simple to implement and highly efficient. The I-V characteristic curve of the PV becomes more complex if the PV receive non-uniform irradiance. A more complex MPPT method like particle swarm optimization is needed [4, 5].

The PV produces heat when electricity is produced. This is based on the normal operating cell temperature (NOCT) test conducted at 800 W/m^2 and 20°C ambient temperature [6]. The PV temperature on average is around 45°C, which is 25°C different from the surrounding. This shows that the energy from the sun is not fully converted into electrical energy and some of the energy is loss in the form of heat. One of the ways to utilize this heat energy is by using the thermoelectric generator (TEG). The TEG is a device that converts heat energy into electrical energy. Since the efficiency of the PV increases as the temperature decreases, absorbing the heat energy from the PV using TEG improves the performance of the PV. Besides that, the electrical energy produced by the TEG also can be used, which further increases the performance of the system. There is research conducted on the PV-TEG cogeneration system (PTCS) [7, 8]. However, this research does not specify any maximization of electrical output since the output is either an open circuit or connected to a dummy load. This is because the TEG has a nonlinear I-V characteristic curve and requires the MPPT method [9, 10].

There are several configurations available for the PTCS. The common practice is the separate boost full MPPT (SBFM) [11-13]. This configuration ensures the MPP is achieved for both PV and TEG. Nonetheless, this configuration requires 2 power converters and 2 MPPT algorithms. This increases the cost of the system. The design is improved by eliminating 1 of the MPPT algorithm. This configuration is called the separate boost partial MPPT (SBPM) [14]. The study shows that the duty cycle of the power converter does not change when operating with the MPPT converter. Therefore, the duty cycle is kept constant and 1 of the MPPT algorithm is removed. The next configuration is the series source boost MPPT (SSBM) [15]. This configuration significantly reduces the cost since the configuration only used 1 boost converter. However, in the study, the performance of the PV and TEG to maximize the power generated is not properly discussed. Another configuration is the PV boost MPPT with series TEG (PBMST) [16]. The TEG is connected in series with the load. Therefore, the power produced by the PV is at an optimum level. The study shows improvement in power production when compared to the PV generation system. Nonetheless, there is no comparison with the other PTCS.

Based on the review, there are several configurations available for the PTCS. However, there is no comparative study presented between these configurations. This is important, especially in the designing phase, where the advantages and disadvantages of each configuration need to be identified. This paper provides a comparative study between 4 configurations of the PTCS. To ensure a fair comparison, all the components used in the study are the same. Only the configuration of the PTCS is changed. The study is fully simulated using MATLAB/Simulink. The boost converters with resistive load are used for the system together with the P&O MPPT method. The effect of heat is neglected in the TEG model.

2.0 METHODOLOGY

Several components are needed in the study. These components include the PV model, TEG model, boost converter, and MPPT. To ensure a fair comparison, the components used in the study are kept constant.

1.1. Photovoltaic Model

The PV model used for the study is the single diode model with series and parallel resistances [17, 18]. The PV current, I_{pv}, is calculated using Equation (1). The parameter of the PV module used in the simulation is listed in Table 1.

Based on the parameters provided by the manufacturer, the theoretical parameter is calculated, which is available in MATLAB/Simulink. The theoretical parameters include the ideality factor (A), thermal voltage (V_t), series resistance (R_s), parallel resistance (R_p), and saturated current (I_s). The temperature of the module, T_m, is calculated using Equation (2), which depends on the ambient temperature (T_a) and irradiance (G).

$$I_{pv} = I_{ph} - I_s\left[\exp\left(\frac{V_{pv} + I_{pv}R_s}{V_t A}\right) - 1\right] - \frac{V_{pv} + I_{pv}R_s}{R_p} \quad (1)$$

$$T_m = T_a + G\left(\frac{NOCT - 20}{800}\right) \quad (2)$$

Table 1 The parameters of the PV model (Advance Solar Hydro Wind Power API-150)

Parameter	Value
Open Circuit Voltage, V_{oc}	41.8 V
Short Circuit Current, I_{sc}	5.05 A
Maximum Power Voltage, V_{mp}	34.5 V
Maximum Power Current, I_{mp}	4.35A
Normal Cell Operating Temperature, $NOCT$	45°C

1.2. Thermoelectric Generator Model

The TEG model is based on Equation (3), in which the TEG voltage, V_{teg}, is calculated based on the TEG current, I_{teg} [19, 20]. Another input for the model is high-temperature side, T_h, and low-temperature side, T_l. The temperature different, dT, is the different between T_h and T_l. The additional parameters are listed in Table 2.

$$V_{teg} = N_s S_{(u)}(T_h - T_l) - \frac{N_{s\_teg}}{N_{p\_teg}} I_{teg} R_{int(u)} \quad (3)$$

Table 2 The parameters of the TEG model

Parameter	Value
Seebeck Coefficient for a Unit Module, $S_{(u)}$	0.015 V/°C
Internal Resistance per Unit Module, $R_{int(u)}$	1.5 Ω
Number of TEG in Series, N_{s_teg}	20
Number of TEG in Parallel, N_{p_teg}	30

1.3. Boost Converter

The boost converter is designed to ensure the operation is in the continuous current mode and within a 1% voltage ripple factor throughout its operation. This is achieved by properly designing the inductance (L), input capacitance (C_i), and output capacitance (C_o). The L, C_i, and C_o are calculated using Equations (4), (5), and (6), respectively [21-23]. The parameters of the boost converter are tabulated in Table 3. The minimum maximum power resistance, $R_{mp(min)}$, is based on PV and TEG during high G. The output resistance, R_o, is adjusted based on the requirement of the configuration.

$$L = \frac{4R_o}{27\gamma_{IL}f} \quad (4)$$

$$C_i = \frac{1 - \sqrt{\frac{R_{mp(min)}}{R_o}}}{8L\gamma_{Vmp}f^2} \quad (5)$$

$$C_o = \frac{1}{\gamma_{Vo}f}\left(\frac{1}{R_o} - \sqrt{\frac{R_{mp(min)}}{{R_o}^3}}\right) \quad (6)$$

Table 3 The parameters of the boost converter

Parameter	Value
Inductance, L	2 mH
Input Capacitance, C_i	200 µF
Output Capacitance, C_o	200 µF
Switching Frequency, f	30 kHz
Inductor Current Ripple Factor, γ_{IL}	20%
Maximum Power Voltage Ripple Factor, γ_{Vmp}	1%
Output Voltage Ripple Factor, γ_{vo}	1%

1.4. Maximum Power Point Tracking

The standard P&O MPPT algorithm is used for all configurations [24, 25]. The algorithm calculated the change of voltage-power (dVP) based on the input voltage (V_i) and input power (P_i) of the boost converter. If the dVP is positive, the duty cycle, D, is reduced. If the dVP is negative, the D is increased. The step of the duty cycle, D_{step}, is kept to 0.2% to minimize the ripple caused by the P&O.

$$dVP(t) = [V_i(t) - V_i(t-1)][P_i(t) - P_i(t-1)] \quad (7)$$

1.5. System Configuration

There are 4 types of configurations analysed for the PTCS. To ensure a fair comparison, the PV model, TEG model, boost converter, and MPPT algorithm is kept identical. The changes are only on the configuration of the load only. The load is changed to ensure the D operates within the desired region, which is 0.0 to 0.8. Further increases the D drops the output voltage, Vo, and leads to failure of the MPPT algorithm. To reduce the complexity of the design, the resistive load is used and separated if 2 boost converters are used.

The first configuration is the SBFM and the block diagram is illustrated in Figure 1(a) [11]. This configuration isolates the PV and TEG. This means that each source has its boost converter and MPPT algorithm. The second configuration is the SBPM and the block diagram is shown in Figure 1(b) [14]. For this configuration, the PV is equipped with a boost converter and MPPT algorithm. However, the MPPT algorithm is replaced with a fixed D, while the boost converter is maintained. A proper D is determined using Equation (8) [21]. The third configuration is the SSBM, which is shown in Figure 1(c) [15]. For this case, both PV and TEG shared the same boost converter and MPPT algorithm. The TEG is connected in series with the PV before being connected to the boost converter. Figure 1(c) shows the fourth configuration, which is called the PBMST [16]. In this configuration, the TEG is connected in series with the load. While the PV is connected at the input of the boost converter with the MPPT algorithm.

$$D = 1 - \sqrt{\frac{R_{mp}}{R_o}} \quad (8)$$

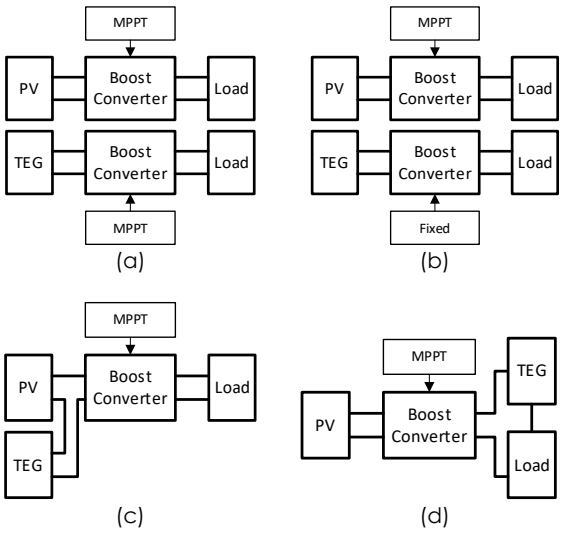

Figure 1 The configurations for the PTCS (a) SBFM; (b) SBPM) [14]; (c) SSBM; [15]. (d) PBMST [16]

The cost of the boost converter and the MPPT needs to be considered during the design. Since the SBFM requires 2 boost converters and 2 MPPTs, the cost of this configuration is the highest among other configurations. The cost for the SBPM is lower than SBFM but higher than the SSBM and PBMST. This is due to the reduction of 1 MPPT controller. The SSBM and PBMST have the lowest cost compared to the SBFM and SBPM. It requires only 1 boost converter and 1 MPPT. Although the cost of the boost converter and MPPT is lower, the cost of the TEG may get high. For this study, the size of the TEG is the same for all configurations. Nonetheless, the size of the TEG can be smaller for the SBFM and SBPM since the PV and TEG is an independent systems. For the SSBM and PBMST, the TEG is affected by the PV. Since both configurations are in series, the I_{pv} equals I_{teg}. Therefore, the N_{p_teg} needs to be appropriate with the PV, for which a proper design is unavailable in the literature and the adjustment needs to be conducted using the try-and-error method. If the is N_{p_teg} too small or too large, the energy from the TEG cannot be extracted. Therefore, the cost may be higher due to the increase in the number of TEG needed to operate properly. Since the input current of the boost converter, I_i, is larger compared to the output current of the boost converter, I_o, the N_{p_teg} for the SSBM is higher compared to the PBMST.

3.0 RESULTS AND DISCUSSION

The simulation aims to determine whether the PV and TEG able to operate at the MPP for each configuration. If the MPP is achieved for the PV and TEG, it means that the configuration fully utilizes the energy generated from these sources. This achievement is observed if the results are close to the MPP. The G starts at 1000 W/m^2, then step-changed to 600 W/m^2, and lastly step-changed to 300 W/m^2. The interval for each change is 1 s. The T_a is kept at 27°C. As a result, the T_m is 59.5°C at 1000 W/m^2, 46.5°C at 600 W/m^2, 36.8°C at 1000 W/m^2. Note that the transient changes in T_m is out of the scope of study.

One of the ways to determine whether the configuration achieved the MPP is by observing the V_{pv} and V_{teg}. The maximum power is extracted from the PV and TEG if the operating voltages are located at the MPP. By referring to Figure 2(a), the V_{pv} can operate near the MPP for all configurations. Nonetheless, this is the opposite of the TEG. The waveforms in Figure 2(b) show that only the SBFM can operate at the MPP. Since the SBFM operate independently, the performance is expected to be quite good. The SBPM is almost close to the MPP. Since the SVPM doesn't have an MPPT algorithm and relies on a fixed D, it is not able to properly adjust its operation at the TEG. As a result, there is a slight error in its operation. The operation of the SSBM and PBMST highly depends on I_{pv} and I_o, respectively. The V_{teg} is higher when the I_{teg} is lower. While the I_o is lower than the I_i for the boost converter. Since the TEG is placed at the input of the boost converter for SSBM and received a high I_{teg}, the SSBM has a lower voltage compared to the PBMST.

The PV power (P_{pv}) and TEG power (P_{teg}) are also observed during the simulation. Similar to the V_{pv}, the P_{pv} is close to MPP at all G. Therefore, the maximum power is extracted from the PV for all configurations, as shown in Figure 3(a). For the TEG, only the SBFM and SBPM can operate close to the MPP based on Figure 3(b). Since the V_{teg} for the SSBM and PBMST is far from the MPP, the P_{teg} also much lower, especially during 1000 W/m^2.

The P-V characteristic curve allows a clearer view of the operation of the PTCS. The P_{pv} and V_{pv} is plotted together to become a power-voltage (P-V) characteristic curve, as shown in Figure 4(a). The result shows that the maximum power able to be extracted from the PV when compared with the PV model. The P_{teg} and V_{teg} are plotted together to become P-V characteristic curve, as shown in Figure 4(b). The results show similar results, in which the SBFM extract the maximum power from the TEG. While the SBPM operate closely to the MPP. While the SSBM and PBMST are far from the MPP.

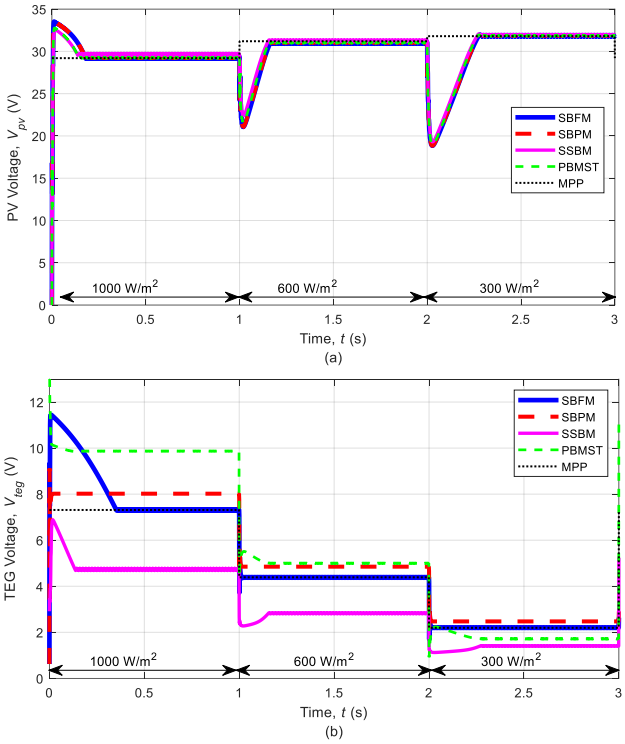

Figure 2 The a) V_{pv} and b) V_{teg} against t for different configurations when the G is stepped changed

The maximum power point efficiency, η_{mpp}, is used to determine whether the configuration can fully extract the energy from the PV and TEG. A higher η_{mpp} shows higher performance. The η_{mpp} of PV(η_{mpp_pv},) and η_{mpp} of TEG (η_{mpp_teg}) are calculated using Equation (9) for the PV and Equation (10), respectively. The η_{mpp_pv} is all above 98.5% regardless of configuration and G, as provided in Figure 5(a). For the η_{mpp_teg}, the SBFM has 99.9% regardless of the G, as shown in Figure 5(b). The η_{mpp_teg} for the SBPM starts with 98.4% at 300 W/m^2, 98.9% at 600 W/m^2, and 99.1% at 1000 W/m^2. The η_{mpp_teg} is still quite high even though there no MPPT algorithm for the TEG. However, based on the calculation of D shown in Equation (8), the D needs to be recalculated when

the R_o changes [21]. If the load is constant, the SBPM is suitable. Nonetheless, if the R_o kept changing, the SBPM is not suitable since the D is required to maintain MPP changes. The η_{mpp} for the PV and TEG, η_{mpp_pvteg}, is calculated using Equation (11) and the result is shown in Figure 5(c). The results show that all configurations can maintain η_{mpp_pvteg} above 98% regardless of the G. This is due to the low power production by the TEG that results in only a minor reduction of η_{mpp_pvteg}.

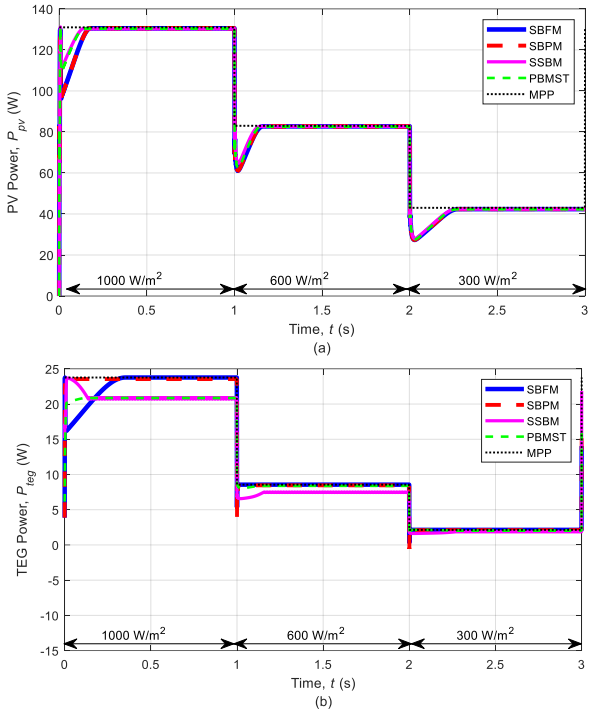

Figure 3 The a) P_{pv} and b) P_{teg} against t for different configurations when the G is stepped changed

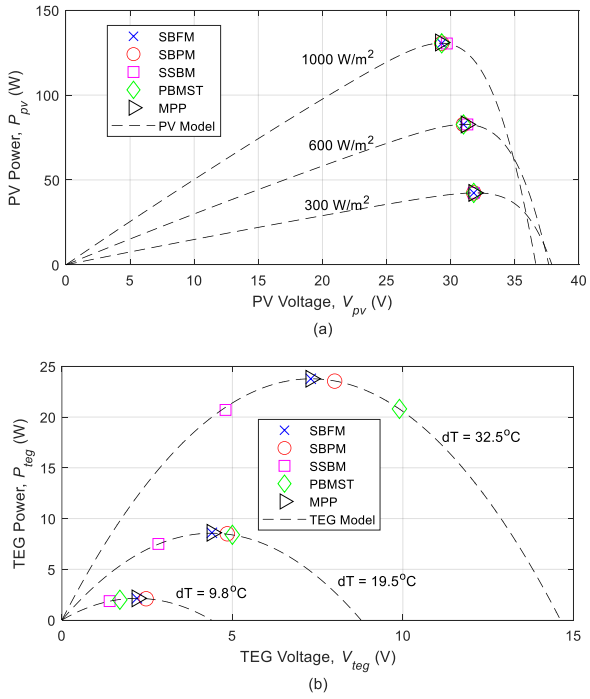

Figure 4 The P-V characteristic curve for different configurations and G

$$\eta_{mpp\_pv} = \frac{P_{pv}}{P_{pv(mpp)}} \times 100\% \quad (9)$$

$$\eta_{mpp\_teg} = \frac{P_{teg}}{P_{teg(mpp)}} \times 100\% \quad (10)$$

$$\eta_{mpp\_pvteg} = \frac{P_{pv} + P_{teg}}{P_{pv(mpp)} + P_{teg(mpp)}} \times 100\% \quad (11)$$

where the $P_{pv(mpp)}$ and $P_{teg(mpp)}$ are the theoretical maximum power point taken from the PV model for PV and TEG, respectively.

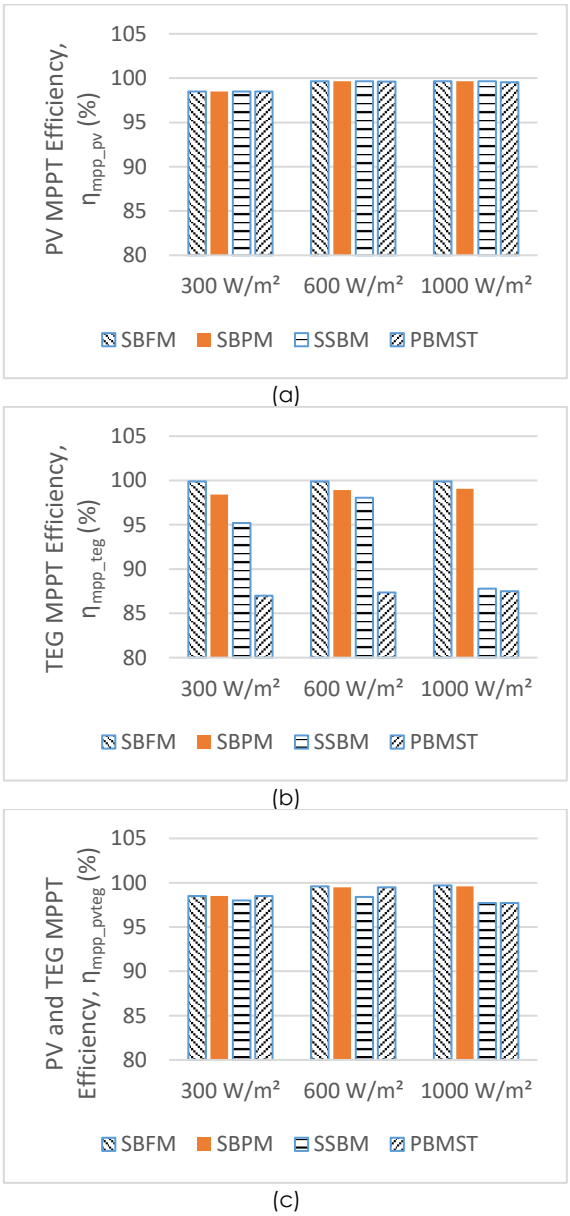

Figure 5 The η_{mpp} for different configurations and G. a) PV. b) TEG. c) PV and TEG

4.0 CONCLUSION

The paper discusses various configurations of the PTCS and its effect on efficiency. The results show that the efficiency of the PV is not affected regardless of its configuration. All configurations can maintain more than 98.5% efficiency. However, the efficiency of the TEG is highly affected by the configurations used. The SBFM configuration can maintain 99% efficiency. While the SBPM configuration can

maintain 98% efficiency if the load does not change during the operation. If the load changes, a new duty cycle needs to be calculated to obtain high efficiency. For the SSBM and PBST configurations, the efficiency is low as 87%. Although the TEG efficiency is lower for these configurations, it does not affect the overall efficiency of the system. This is due to the relatively low power production when compared to the PV power output. In conclusion, the configuration chosen affects the efficiency of the TEG. Nonetheless, the efficiency of the PV and PV-TEG is not significantly affected by the configuration.

Conflicts of Interest

The author(s) declare(s) that there is no conflict of interest regarding the publication of this paper.

Acknowledgement

This research was supported by Ministry of Higher Education (MOHE) through Fundamental Research Grant Scheme (FRGS/1/2021/TK0/UTM/02/19). The authors would like to express gratitude to Universiti Teknologi Malaysia (UTM) for providing comprehensive facilities. Lastly, thanks to colleagues who have either directly or indirectly contributed to the completion of this work.

References

[1] REN21. 2023. Renewables 2022 Global Status Report (GSR). Renewable Energy Policy Network for the 21st Century (REN21).

[2] A. H. Mutlag, A. Mohamed, and H. Shareef. 2016. An Improved Perturbation and Observation Based Maximum Power Point Tracking Method for Photovoltaic Systems. *Jurnal Teknologi.* 78(6-2): 06/05. Doi: 10.11113/jt.v78.8887.

[3] S. C. Wang, H. Y. Pai, G. J. Chen, and Y. H. Liu. 2020. A Fast and Efficient Maximum Power Tracking Combining Simplified State Estimation With Adaptive Perturb and Observe. *IEEE Access*. 8: 155319-155328. Doi: 10.1109/ACCESS.2020.3019197.

[4] A. Ballaji, R. Dash, V. Subburaj, J. R. Kalvakurthi, D. Swain, and S. C. Swain. 2022. Design & Development of MPPT Using PSO With Predefined Search Space Based on Fuzzy Fokker Planck Solution. *IEEE Access*. 10: 80764-80783. Doi: 10.1109/ACCESS.2022.3195036.

[5] N. Priyadarshi, S. Padmanaban, J. B. Holm-Nielsen, F. Blaabjerg, and M. S. Bhaskar. 2020. An Experimental Estimation of Hybrid ANFIS–PSO-Based MPPT for PV Grid Integration Under Fluctuating Sun Irradiance. *IEEE Systems Journal.* 14(1): 1218-1229. Doi: 10.1109/JSYST.2019.2949083.

[6] J. H. Bae, D. Y. Kim, J. W. Shin, S. E. Lee, and K. C. Kim. 2020. Analysis on the Features of NOCT and NMOT Tests With Photovoltaic Module. *IEEE Access*. 8: 151546-151554. Doi: 10.1109/ACCESS.2020.3017372.

[7] M. Sabry, A. Lashin, and M. Al Turkestani. 2021. Experimental and Simulation Investigations of CPV/TEG Hybrid System. *Journal of King Saud University - Science*. 33(2): 101321. Doi: https://doi.org/10.1016/j.jksus.2020.101321.

[8] C. Babu and P. Ponnambalam. 2018. The Theoretical Performance Evaluation of Hybrid PV-TEG System. *Energy Conversion and Management*. 173: 450-460. Doi: https://doi.org/10.1016/j.enconman.2018.07.104.

[9] M. R. Ariffin, S. Shafie, W. Z. W. Hassan, N. Azis, and M. E. Ya'acob. 2017. Conceptual Design of Hybrid Photovoltaic-thermoelectric Generator (PV/TEG) for Automated Greenhouse System. *2017 IEEE 15th Student Conference on Research and Development (SCOReD)*. 309-314. Doi: 10.1109/SCORED.2017.8305373.

[10] S. Koushik, S. Das, V. Sharma, P. Walde, and N. Maji. 2018. PV and TEG Hybrid Power Generation for Enhancement of Efficiency. *2018 8th IEEE India International Conference on Power Electronics (IICPE)*. 1-6. Doi: 10.1109/IICPE.2018.8709422.

[11] V. Verma, A. Kane, and B. Singh. 2016. Complementary Performance Enhancement of PV Energy System through Thermoelectric Generation. *Renewable and Sustainable Energy Reviews.* 58: 1017-1026. Doi: https://doi.org/10.1016/j.rser.2015.12.212.

[12] B. A, C. I, K. K, B. R, and B. H. I. 2018. Maximum Power Extraction from a Photovoltaic Panel and a Thermoelectric Generator Constituting a Hybrid Electrical Generation System. *2018 International Conference on Smart Grid (icSmartGrid)*, 4-6 Dec. 2018. 276-282. Doi: 10.1109/ISGWCP.2018.8634534.

[13] T. H. Kwan and X. Wu. 2017. The Lock-On Mechanism MPPT Algorithm as Applied to the Hybrid Photovoltaic Cell and Thermoelectric Generator System. *Applied Energy*. 204: 873-886. Doi: https://doi.org/10.1016/j.apenergy.2017.03.036.

[14] K. N. 2021. Photovoltaic and Thermoelectric Generator Combined Hybrid Energy System with an Enhanced Maximum Power Point Tracking Technique for Higher Energy Conversion Efficiency.*Sustainability*. 13(6): 3144. https://www.mdpi.com/2071-1050/13/6/3144.

[15] H. Rezk, Z. M. Ali, O. Abdalla, O. Younis, M. R. Gomaa, and M. Hashim. 2019. Hybrid Moth-Flame Optimization Algorithm and Incremental Conductance for Tracking Maximum Power of Solar PV/Thermoelectric System under Different Conditions. *Mathematics.* 7(10): 875. https://www.mdpi.com/2227-7390/7/10/875.

[16] N. Kanagaraj and H. Rezk. 2021. Dynamic Voltage Restorer Integrated with Photovoltaic-Thermoelectric Generator for Voltage Disturbances Compensation and Energy Saving in Three-Phase System. *Sustainability*. 13(6): 3511. https://www.mdpi.com/2071-1050/13/6/3511.

[17] R. Ayop and C. W. Tan. 2016. A Comparison Study of Interpolation and Circuit based Photovoltaic Mathematical Models. *2016 IEEE International Conference on Power and Energy (PECon)*, 28-29 Nov. 2016. 626-631. Doi: 10.1109/PECON.2016.7951636.

[18] A. Fudholi, M. Zohri, I. Taslim, M. A. Indrianti, and I. N. Manyoe. 2020. Theoretical Approach Model of Building Integrated Photovoltaic Thermal Air Collector. *International Journal of Power Electronics and Drive Systems.* 2: 1002.

[19] R. Ayop, C. W. Tan, A. L. Bukar, A. Jusoh, N. D. Muhamad, and S. N. S. Nasir. 2022. The Design of Energy Storage based on Thermoelectric Generator and bidirectional Converter. *International Journal of Power Electronics and Drive Systems (IJPEDS)*. 13(3): 1605-1613. Doi: 10.11591/ijpeds.v13.i3.pp1605-1613

[20] M. Alian Fini, D. Gharapetian, and M. Asgari. 2022. Efficiency Improvement of Hybrid PV-TEG System based on an Energy, Exergy, Energy-economic and Environmental Analysis; Experimental, Mathematical and Numerical Approaches. *Energy Conversion and Management*. 265: 115767. Doi: https://doi.org/10.1016/j.enconman.2022.115767.

[21] R. Ayop and C. W. Tan. 2018. Design of Boost Converter based on Maximum Power Point Resistance for Photovoltaic Applications. *Solar Energy*. 160: 322-335. Doi: https://doi.org/10.1016/j.solener.2017.12.016.

[22] H. Jedi and G. A. Hussain. 2022. A 1 MHz Soft-switching Boost DC-DC Converter with Matching Network. *International Journal of Power Electronics and Drive Systems.* 13(4): 2226.

[23] D. W. Hart. 2011. *Power Electronics*. Valparaiso University, Indiana: Tata McGraw-Hill Education.

[24] R. Ayop, M. F. I. Zaki, C. W. Tan, S. Md Ayob, and M. J. Abdul Aziz. 2022. Optimum Sizing of Components for Photovoltaic Maximum Power Point Tracking Buck Converter. *Solar Energy*. 243: 236-246. Doi: https://doi.org/10.1016/j.solener.2022.07.032.

[25] H. Attia and S. Ulusoy. 2021. A new Perturb and Observe MPPT Algorithm based on Two Steps Variable Voltage control. *International Journal of Power Electronics and Drive Systems.* 12(4): 2201.